ChemComm

RSC Publishing

COMMUNICATION

View Article Online
View Journal | View Issue

Side chain and backbone structure-dependent subcellular localization and toxicity of conjugated polymer nanoparticles†

Cite this: *Chem. Commun.*, 2013, **49**, 6048

Received 23rd April 2013,
Accepted 16th May 2013

DOI: 10.1039/c3cc43015d

www.rsc.org/chemcomm

Eladio Mendez and Joong Ho Moon*

The subcellular localization and toxicity of conjugated polymer nanoparticles (CPNs) are dependent on the chemical structure of the side chains and backbone. Primary amine-containing CPNs exhibit high Golgi localization with no toxicity. Incorporation of short ethylene oxide and tertiary amine side chains contributes to decreased Golgi localization and increased toxicity, respectively.

Semiconducting conjugated polymer nanoparticles (CPNs) and conjugated polyelectrolytes (CPEs) are emerging fluorescent biomaterials for cellular labelling,[1] sensing,[2] therapeutics,[3] and delivery[4] of biological substances. Excellent photophysical properties of conjugated polymers (CPs) including high molar absorptivity, quantum yield, and energy transfer efficiency make them suitable for various biological applications.[5] Well-established synthetic methods also allow facile modifications of both π-electron conjugated backbones and side chains with various sensing or targeting units. By treating non-aqueous soluble CPs under various particle formation conditions, non-toxic soft nanoparticles have been fabricated and used for cellular labelling and nucleic acid delivery.[6]

Understanding cellular interactions and entry pathways of CPNs is paramount to improving the overall labelling and delivery efficiency. Depending on the entry pathways, the materials and their payloads (*i.e.*, drugs or genes) will be trafficked into different organelles, which will significantly influence the overall efficiency.[7] For example, carriers entrapped in endosomes or lysosomes trafficked *via* a certain type of endocytosis will experience recycling of the contents back to the cell surface and degradation processes in acidic lysosomes, lowering the overall labelling and delivery efficiency.[8] Meanwhile, exogenous materials trafficked by non-destructive organelles such as caveosomes to the Golgi apparatus (*i.e.*, caveolae-mediated endocytosis) have high intracellular retention.[9] Delivery *via* macropinocytosis can also avoid lysosomal degradation routes because macropinosomes do not fuse with the lysosomes, and the membranes of macropinosomes are highly leaky.[10] Therefore, systematic investigation to understand and modulate the cellular interaction and pathways will have a significant impact on designing efficient labelling and delivery vehicles.

Previously, we demonstrated that CPNs fabricated by treating a CP containing both short ethylene oxide (EO) and primary amine (*e.g.*, **P1**, Fig. 1) with organic acids followed by dialysis exhibit efficient cellular labelling and delivery of small interfering RNA without toxic effects.[4a,b] Mechanistic studies further indicate that CPNs use both energy dependent and independent entry pathways. Among the energy dependent pathways, CPNs enter cancer cells *via* caveolae-mediated endocytosis as one of the entry pathways.[11] It is not clear why the CPNs use the specific entry pathway, however, the positive charges and hydrophobicity of CPNs play important roles in interaction with various serum proteins and the cell membranes, which will significantly influence the subsequent cellular uptake.[12] It is also known that materials having high surface-to-volume ratios exhibit size, shape, and functional group-dependent cellular interactions and subsequent entry.[13]

Based on the results and observations, we hypothesized that chemical modifications in the side chains of CPs will change

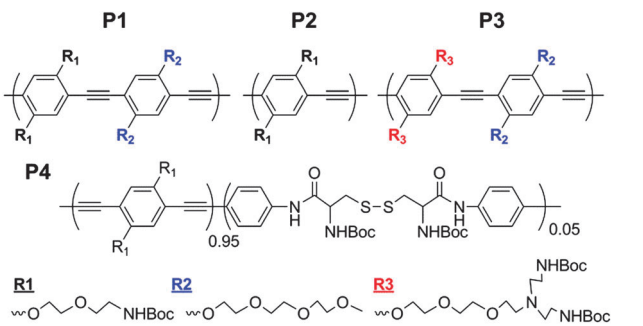

Fig. 1 Chemical structures of CPs. Poly(*p*-phenyleneethynylenes) (PPEs) with different side chains (**P1–P3**) and poly(*p*-phenylenebutadiynylene) (PPB) containing a small amount of flexible unit in the backbone (**P4**) were synthesized and compared for cellular behaviour.

Department of Chemistry and Biochemistry, Florida International University, 11200 SW 8th St., Miami, FL, 33199, USA. E-mail: jmoon@fiu.edu; Tel: +1-305-348-1368

† Electronic supplementary information (ESI) available: Detailed synthetic procedures, characterization, and co-localization analyses. See DOI: 10.1039/c3cc43015d

the subcellular localization of CPNs, because the modulated surface properties will influence the cellular interactions of CPNs and their subsequent entry into cells.

To test the hypothesis, we synthesized four CPNs with different side chain (**P1–P3**) and backbone (**P4**) structures (Fig. 1). Since the cellular interactions and entry processes of nanomaterials are collectively influenced by the physicochemical properties, it is important to keep other physicochemical properties constant when a specific parameter is tested. Because of the particle formation mechanism (*i.e.*, molecular weight independent phase inverse precipitation driven by aqueous insolubility of CPs),[14] the shapes and hydrodynamic radii of CPNs are relatively constant.[15] **CPN-2** was designed and synthesized to check the EO side chain effects on the toxicity and localization by removing the EO unit from the repeating unit of **CPN-1**. **CPN-3** was synthesized to increase amine density using branched amine side chains containing tertiary amines. **CPN-4** was synthesized to compare the backbone flexibility effects while amine density was maintained close to that of **CPN-2**. Synthesis of **P4** was reported in our recent publication.[16] All polymers were treated with a series of organic acids followed by dialysis, affording CPNs that are physically stable in water. Physicochemical properties of CPNs are listed in Table 1. Since aggregation behaviour is concentration dependent, the concentrations of all CPN solutions were adjusted to be 0.5 mM. Non-EO containing **CPN-2** and **CPN-4** exhibited slightly larger hydrodynamic radii than those of **CPN-1** and **CPN-3** fabricated with EO containing polymers. The difference in hydrodynamic radius among the CPNs is expected to have minimal effects on the cellular interaction and subcellular localization due to the polydisperse nature of CPNs. Zeta potentials of CPNs were determined to be ~+42–46 mV, except for **CPN-1** exhibiting ~+20 mV (Table 1).

To test how the side chain structure influences cellular toxicity, CPNs were incubated with human cervical carcinoma cells (HeLa) overnight at various concentrations. Zeta potentials of CPNs had no direct correlation with the toxicity, but the chemical structure (*i.e.*, type and density of amine) of the side chains was related to the cellular toxicity. As shown in Fig. 2, **CPN-3** containing the highest amine density, including tertiary amines, exhibited substantial toxicity starting from 10 μM, while no cell viability inhibition was observed up to 40 μM for the primary amine containing CPNs, whether they contain EO side chains or flexible backbones (*i.e.*, **CPN-1**, **-2**, and **-4**). Compared to **CPN-2**, which contains the same amount of primary amines per repeating unit as **CPN-3**, toxicity of **CPN-3** can be attributed to both increased amine density and the high buffering capacity of tertiary amines. Membrane disruption properties of synthetic carriers containing tertiary amines have been used to increase payload escape from the endosomes or lysosomes, however, these classes of materials often cause toxicity issues.[17]

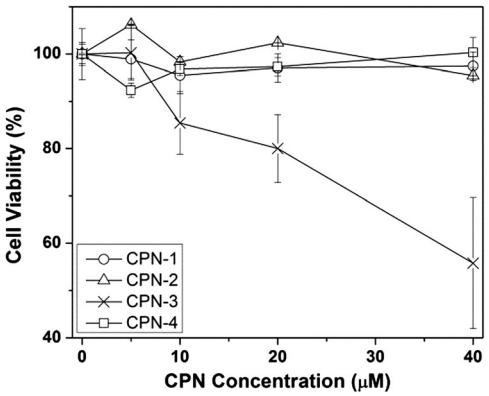

Fig. 2 Cellular toxicity of CPNs measured by cell viability inhibition at various concentrations.

Subcellular localization of CPNs was monitored by fluorescent microscopic imaging. HeLa cells incubated with CPNs (green) overnight were co-stained with pHRhodo Dextran (10 kDa) (red) and BODIPY-TR C5-ceramide–BSA complex (red) for labelling acidic organelles (*i.e.*, endosomes and lysosomes) and Golgi apparatus, respectively (Fig. 3a and ESI†). CPNs were mainly found at the perinuclear regions (punctuated green dots) and exhibited overlaps with both pHRhodo and BODIPY. Co-localization patterns with the Golgi were clearly distinguishable among CPNs having different side chain or backbone structures (Fig. 3a), while overlapping patterns with pHRhodo were relatively uniform (ESI†). **CPN-2** and **CPN-4**, which only contain primary amine side chains, exhibit high Golgi localization (Fig. 3a), while **CPN-1** and **CPN-3**, which contain both EO and amine side chains, exhibit a relatively low Golgi overlap.

To obtain quantitative co-localization information, all images were further analysed using Pearson's Correlation Coefficient (PCC) method. The PCC method gauges the level of overlap by measuring the pixel-by-pixel covariance in the signals of two images. Because the PCC method uses normalized signals by subtracting the mean intensity from each pixel's intensity value, PCC is independent of signal levels (probe brightness) and signal offset (background).[18] PCC values of 0 and 1 correspond to uncorrelated and perfectly linear correlated images, respectively. Instead of picking small, subjective regions of interest within an

Table 1 Physicochemical properties of CPNs

CPN	Type	M_n[a] (kDa)	PDI[b]	$\lambda_{max,abs}$[c] (nm)	$\lambda_{max,em}$[d] (nm)	Hydrodynamic radius[e] (nm)	PDI[e]	Zeta potential[f] (mV)
1	**P1** (PPE)	16.4	1.49	433	496	61 ± 6.7	0.27 ± 0.02	+20 ± 0.4
2	**P2** (PPE)	11.8	1.43	427	492	71 ± 7.9	0.29 ± 0.02	+42 ± 5.1
3	**P3** (PPE)	10.7	1.64	420	496	58 ± 3.4	0.33 ± 0.06	+44 ± 1.1
4	**P4** (PPB)	22.3	2.28	444	500	87 ± 6.1	0.51 ± 0.03	+46 ± 2.3

[a] Determined by gel permeation chromatography in THF relative to polystyrene standard. [b] Polydispersity index (PDI) = M_w/M_n. [c] Measured in water. [d] Measured in water, excitation wavelength 400 nm. [e] Measured by DLS at 500 μM in water. Mean ± standard deviation. [f] Electrophoretic measurement at pH 7.0. Mean ± standard deviation.

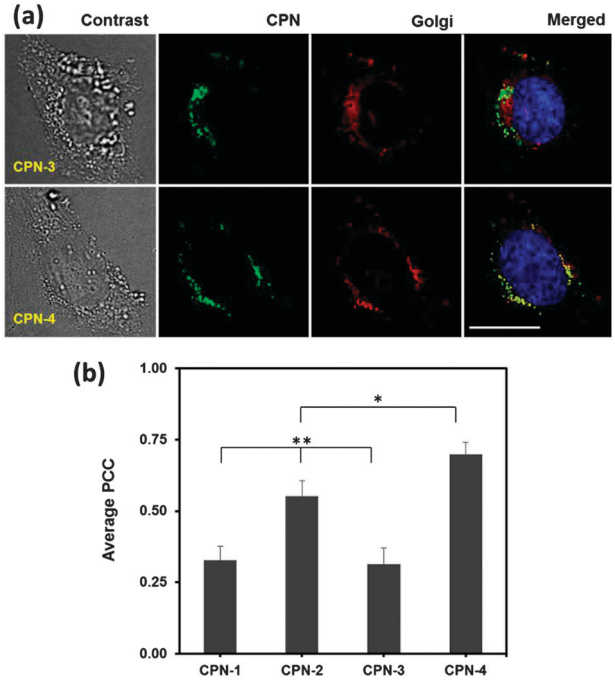

Fig. 3 (a) Microscopic images of HeLa cells incubated with **CPN-3** and **CPN-4**, followed by Golgi (red) and nucleus (blue) staining. The scale bar is 20 μm. **CPN-4** exhibits higher overlap with Golgi than **CPN-3**. (b) Quantitative analysis of co-localization using the PCC algorithm. Co-localization with Golgi is dependent on the side chain and backbone structures. The error bar represents ±standard deviation (n = 3). * < 0.05 when **CPN-4** compared with **CPN-2**. ** < 0.0005 when **CPN-1** and **CPN-3** compared with **CPN-2** and **CPN-4** (n = 3).

image, three independent images of an entire cell were selected and analysed to increase the analysis objectivity. As shown in Fig. 3b, average PCC values were dependent on the side chain and backbone structures of the CPNs. The CPNs with only amine side chains exhibited higher Golgi localization than the CPNs containing both EO and amine side chains. In addition, CPNs fabricated with a semi-flexible CP exhibited the highest Golgi localization. One-way ANOVA followed by the Tukey mean separation method confirmed that Golgi co-localization of **CPN-2** and **CPN-4** was statistically significant ($p < 0.003$) than that of **CPN-1** and **CPN-3**. The Golgi co-localization between **CPN-2** and **CPN-4** was also statistically significant ($p < 0.05$).

In conclusion, we have demonstrated that CPNs are promising biomaterials with tunable physicochemical properties. The side chain and backbone structures of CPNs are closely related to toxicity and subcellular localization. Therefore, cellular interaction and cellular entry pathways of CPNs can be fine-tuned to improve labelling and delivery efficiency. The excellent intrinsic fluorescent nature of CPNs, which are useful for labelling and monitoring biological substances, the tunable physicochemical properties and the related biophysical properties make CPNs excellent biomaterials. The concept we demonstrated here will lead to the development of novel multifunctional materials for labelling, sensing, and delivery. Using the highly non-destructive delivery pathway and biodegradability of **CPN-4**, we are currently investigating the delivery of small RNA molecules to target cells.

This work was supported by National Institute of Health/ National Institute of General Medical Sciences Grant No. SC1GM092778 and R25GM61347.

Notes and references

1 I. B. Kim, H. Shin, A. J. Garcia and U. H. F. Bunz, *Bioconjugate Chem.*, 2007, **18**, 815; X. L. Feng, Y. L. Tang, X. R. Duan, L. B. Liu and S. J. Wang, *Mater. Chem.*, 2010, **20**, 1312; K. Lee, J. Lee, E. J. Jeong, A. Kronk, K. S. J. Elenitoba-Johnson, M. S. Lim and J. Kim, *Adv. Mater.*, 2012, **24**, 2479; C. F. Wu and D. T. Chiu, *Angew. Chem., Int. Ed.*, 2013, **52**, 3086.
2 M. D. Disney, J. Zheng, T. M. Swager and P. H. Seeberger, *J. Am. Chem. Soc.*, 2004, **126**, 13343; C. H. Fan, S. Wang, J. W. Hong, G. C. Bazan, K. W. Plaxco and A. J. Heeger, *Proc. Natl. Acad. Sci. U. S. A.*, 2003, **100**, 6297; H. A. Ho, K. Dore, M. Boissinot, M. G. Bergeron, R. M. Tanguay, D. Boudreau and M. J. Leclerc, *J. Am. Chem. Soc.*, 2005, **127**, 12673; K. E. Achyuthan, T. S. Bergstedt, L. Chen, R. M. Jones, S. Kumaraswamy, S. A. Kushon, K. D. Ley, L. Lu, D. McBranch, H. Mukundan, F. Rininsland, X. Shi, W. Xia and D. G. J. Whitten, *Mater. Chem.*, 2005, **15**, 2648; C. J. Sun, B. S. Gaylord, J. W. Hong, B. Liu and G. C. Bazan, *Nat. Protocols*, 2007, **2**, 2148; B. Liu and G. C. Bazan, *Chem. Mater.*, 2004, **16**, 4467.
3 Y. Wang, S. D. Jett, J. Crum, K. S. Schanze, E. Y. Chi and D. G. Whitten, *Langmuir*, 2013, **29**, 781; C. L. Zhu, Q. Yang, F. T. Lv, L. B. Liu and S. Wang, *Adv. Mater.*, 2013, **25**, 1203; C. F. Xing, L. B. Liu, H. W. Tang, X. L. Feng, Q. Yang, S. Wang and G. C. Bazan, *Adv. Funct. Mater.*, 2011, **21**, 4058.
4 (*a*) J. H. Moon, E. Mendez, Y. Kim and A. Kaur, *Chem. Commun.*, 2011, **47**, 8370; (*b*) A. T. Silva, N. Alien, C. M. Ye, J. Verchot and J. H. Moon, *BMC Plant Biol.*, 2010, **10**, 291; X. L. Feng, F. T. Lv, L. B. Liu, Q. Yang, S. Wang and G. C. Bazan, *Adv. Mater.*, 2012, **24**, 5428.
5 S. W. Thomas, G. D. Joly and T. M. Swager, *Chem. Rev.*, 2007, **107**, 1339; C. L. Zhu, L. B. Liu, Q. Yang, F. T. Lv and S. Wang, *Chem. Rev.*, 2012, **112**, 4687.
6 J. H. Moon, W. McDaniel, P. MacLean and L. E. Hancock, *Angew. Chem., Int. Ed.*, 2007, **46**, 8223; C. F. Wu, C. Szymanski and J. McNeill, *Langmuir*, 2006, **22**, 2956; M. C. Baier, J. Huber and S. J. Mecking, *J. Am. Chem. Soc.*, 2009, **131**, 14267.
7 R. Duncan and S. C. W. Richardson, *Mol. Pharmaceutics*, 2012, **9**, 2380; G. Sahay, D. Y. Alakhova and A. V. J. Kabanov, *J. Controlled Release*, 2010, **145**, 182.
8 J. Rejman, A. Bragonzi and M. Conese, *Mol. Ther.*, 2005, **12**, 468.
9 L. Pelkmans and A. Helenius, *Traffic*, 2002, **3**, 311.
10 I. A. Khalil, K. Kogure, S. Futaki and H. Harashima, *J. Biol. Chem.*, 2006, **281**, 3544.
11 J. Lee, M. Twomey, C. Machado, G. Gomez, M. Doshi, A. J. Gesquiere and J. H. Moon, *Macromol. Biosci.*, DOI: 10.1002/mabi.201300030.
12 A. E. Nel, L. Madler, D. Velegol, T. Xia, E. M. V. Hoek, P. Somasundaran, F. Klaessig, V. Castranova and M. Thompson, *Nature Mater.*, 2009, **8**, 543; L. P. Fernando, P. K. Kandel, J. Yu, J. McNeill, P. C. Ackroyd and K. A. Christensen, *Biomacromolecules*, 2010, **11**, 2675.
13 S. J. Tan, N. R. Jana, S. J. Gao, P. K. Patra and J. Y. Ying, *Chem. Mater.*, 2010, **22**, 2239.
14 Y. J. Ko, E. Mendez and J. H. Moon, *Macromolecules*, 2011, **44**, 5527.
15 Pancake-like shapes of CPNs on a mica surface were observed from atomic force microscopy images. See *Macromol. Biosci.*, 2013, DOI: 10.1002/mabi.201300030.
16 T. Vokatá and J. H. Moon, *Macromolecules*, 2013, **46**, 1253.
17 C.-C. Lee, Y. Liu and T. M. Reineke, *Bioconjugate Chem.*, 2008, **19**, 428.
18 K. W. Dunn, M. M. Kamocka and J. H. McDonald, *Am. J. Physiol.: Cell Physiol.*, 2011, **300**, C723.

